

## DNA Origami as a Carrier for Circumvention of Drug Resistance

Qiao Jiang,<sup>†</sup> Chen Song,<sup>†</sup> Jeanette Nangreave,<sup>‡</sup> Xiaowei Liu,<sup>‡</sup> Lin Lin,<sup>§</sup> Dengli Qiu,<sup>#</sup> Zhen-Gang Wang,<sup>†</sup> Guozhang Zou,<sup>†</sup> Xingjie Liang,<sup>†</sup> Hao Yan,<sup>\*,‡</sup> and Baoquan Ding<sup>\*,†</sup>

<sup>†</sup>National Center for NanoScience and Technology, 11 BeiYiTiao, ZhongGuanCun, 100190 Beijing, China

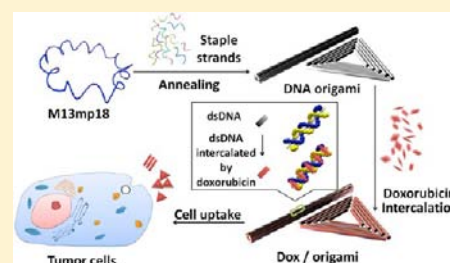
<sup>‡</sup>Department of Chemistry and Biochemistry & the Biodesign Institute, Arizona State University, Tempe, Arizona 85287, United States

<sup>§</sup>Cancer Institute & Hospital, PUMC & CAMS of China, 100021 Beijing, China

<sup>#</sup>Buker Nano Surfaces, 11 ZhongGuanCun South Street, 100081 Beijing, China

### **S** Supporting Information

**ABSTRACT:** Although a multitude of promising anti-cancer drugs have been developed over the past 50 years, effective delivery of the drugs to diseased cells remains a challenge. Recently, nanoparticles have been used as drug delivery vehicles due to their high delivery efficiencies and the possibility to circumvent cellular drug resistance. However, the lack of biocompatibility and inability to engineer spatially addressable surfaces for multi-functional activity remains an obstacle to their widespread use. Here we present a novel drug carrier system based on self-assembled, spatially addressable DNA origami nanostructures that confronts these limitations. Doxorubicin, a well-known anti-cancer drug, was non-covalently attached to DNA origami nanostructures through intercalation. A high level of drug loading efficiency was achieved, and the complex exhibited prominent cytotoxicity not only to regular human breast adenocarcinoma cancer cells (MCF 7), but more importantly to doxorubicin-resistant cancer cells, inducing a remarkable reversal of phenotype resistance. With the DNA origami drug delivery vehicles, the cellular internalization of doxorubicin was increased, which contributed to the significant enhancement of cell-killing activity to doxorubicin-resistant MCF 7 cells. Presumably, the activity of doxorubicin-loaded DNA origami inhibits lysosomal acidification, resulting in cellular redistribution of the drug to action sites. Our results suggest that DNA origami has immense potential as an efficient, biocompatible drug carrier and delivery vehicle in the treatment of cancer.



### ■ INTRODUCTION

Doxorubicin, one of the most well-known chemotherapy drugs, is used to treat a wide range of cancers by intercalating DNA and inhibiting macromolecular biosynthesis.<sup>1–3</sup> Like other traditional anti-cancer drugs, it has a variety of drawbacks including adverse side effects, poor selectivity, and accumulation in tumors.<sup>3–5</sup> Moreover, doxorubicin has been shown to induce multi-drug resistance in cancer cells, both in laboratory investigations and in clinical studies.<sup>4,5</sup> There are a variety of mechanisms by which cancer cells become resistant to anti-cancer treatments, the most common of which is the detection and subsequent ejection of the drugs from cells.<sup>4,5</sup> Other mechanisms of drug resistance include the loss of a cell surface receptor or transporter for a drug, compartmentalization of a drug by vesicular organelles, and specific metabolism of a drug.<sup>5</sup>

Nanoscale anti-cancer agents have emerged as a promising new class of cancer therapeutics. Early clinical results suggest that nanoparticles (NPs) exhibit enhanced delivery efficiencies and reduced side effects due to more accurate localization in tumors and more active cellular uptake.<sup>6–9</sup> Nanocontainers for drug delivery are also attracting significant attention because the use of an appropriate drug delivery vehicle can significantly increase the likelihood that a drug is efficiently delivered and taken up by cells. The most commonly used nanocontainers for

hosting therapeutic cargoes, e.g., small-molecule drugs, peptides, proteins, and nucleic acids, are formed from lipids and polymers.<sup>6–9</sup> The first generation of NP drug delivery systems is already in use; for example, Doxil (Ortho Biotech), a PEGylated liposomal formulation for doxorubicin, has been used in a clinical setting for over two decades.<sup>7</sup> Unfortunately, it causes only a modest increase in anti-tumor activity due to the slow release of doxorubicin from the liposomal sheaths.<sup>10,11</sup> Metal NPs have also been targeted as promising drug-delivery vehicles; gold NPs have already been used for the controlled release of chemotherapy drugs.<sup>12</sup> Although metal NPs are both biocompatible and chemically inert, they may be retained in the body long after administration of the drug, and accumulation of metal NPs can lead to toxicity.<sup>9</sup> Thus, it remains a challenge to develop safe, biocompatible, and effective nanocarriers for drug delivery.

With a high level of structural programmability and obvious biocompatibility, self-assembled DNA nanostructures are among the most promising candidates to serve as nanocarriers for drug delivery. It is relatively easy to construct complex DNA nanostructures with precisely defined shapes and dimensions

Received: May 3, 2012

Published: July 17, 2012

using rational design principles.<sup>13–24</sup> In particular, the DNA origami method produces fully addressable structures in extremely high yields.<sup>13</sup> In this method, a long single strand of DNA (scaffold strand, usually viral genomic DNA) is folded into arbitrary shapes by hundreds of short strands (staples, synthetic oligonucleotides). In addition to holding the scaffold in place, the staples provide addressable units for functionalization by various biomolecules and NPs.<sup>25–29</sup> These modifications can be used to facilitate imaging, targeted delivery, and controlled release of therapeutic compounds. Consequently, the potential of DNA origami structures for nanomedical applications has gained great interest.<sup>30–32</sup>

Recent studies have shown that DNA macromolecules do not exhibit any obvious cytotoxicity or immunogenicity, both of which are important features of effective drug delivery vehicles.<sup>31–33</sup> DNA origami structures were also found to be very stable in cell lysate,<sup>35</sup> a prerequisite for controlled release of a drug to subcellular targets. One of the first demonstrations of a DNA nanostructure-based drug delivery platform was reported by Chang et al., who developed doxorubicin aptamer-conjugated DNA icosahedra that demonstrated efficient killing of cancer cells.<sup>34</sup> Scaffolded DNA origami has an even greater potential to deliver therapeutic levels of doxorubicin than polyhedral wireframe structures because the additional layers of tightly packed double-helices provide many more docking sites for intercalation. The high density of doxorubicin can offset the effects of enzymatic degradation and the unintended release of the drug.

Here we report the construction of two- and three-dimensional doxorubicin-loaded DNA origami structures. The DNA nanostructure–doxorubicin complexes were administered to regular human breast adenocarcinoma cancer cells MCF 7 (reg-MCF 7) and a cell subline that is doxorubicin-resistant (res-MCF 7). The cytotoxicity of origami-bound doxorubicin and free doxorubicin to reg-MCF 7 and res-MCF 7 cells was evaluated. To clarify a possible mechanism of cell death, we investigated the internalization effect of doxorubicin by drug-loaded DNA carriers and the influence on cellular lysosomal pH value.

## METHODS

**Materials.** All oligonucleotides were purchased from Integrated DNA Technologies or Invitrogen China. The origami staple strands were stored in 96-well plates with concentrations normalized to 100  $\mu\text{M}$  and used without further purification. The concentration of each strand was estimated by measuring the UV absorbance at 260 nm. M13 viral DNA was purchased from New England Biolabs, Inc. (single-strand DNA, N4040S; double-strand RF I DNA, N4018S). Doxorubicin was purchased from Beijing Huafeng United Technology (China).

**Self-Assembly of DNA Origami.** Triangular- and tubular-shaped DNA origami structures were assembled according to Rothmund's and Yan's methods.<sup>13,36</sup> A molar ratio of 1:10 between the long viral ssDNA M13mp18 (5 nM) and the short helper strands (unpurified) was used. DNA origami was assembled in  $1\times$  TAE/Mg<sup>2+</sup> buffer (Tris, 40 mM; acetic acid, 20 mM; EDTA, 2 mM; and magnesium acetate, 12.5 mM; pH 8.0) by slowly cooling from 90 °C to room temperature.

**Characterization of DNA Origami.** Agarose gel electrophoreses was performed at room temperature (1%, stained with ethidium bromide), and the images were collected by a gel imaging system (GE). Typically, AFM imaging of DNA nanostructures is performed in tapping-in-buffer mode. Here, for both DNA origami structures and drug-loaded DNA origami structures, 5  $\mu\text{L}$  of sample was deposited on mica and left to adsorb to the surface for 20 min. The sample was subsequently washed with ddH<sub>2</sub>O three times, and TAE/Mg<sup>2+</sup> buffer

was added for imaging (Baker Nano Surfaces Beijing Representative Office, China).

**Doxorubicin Loading.** Doxorubicin solution (2 mM) was incubated with the DNA origami structures (triangle or tube, 2.5 nM) or double-strand M13 DNA (2.5 nM) for 24 h and then centrifuged at 10 000 rpm at room temperature for 10 min. After centrifuging, the dark red precipitate (drug-loaded origami or drug-loaded ds M13 DNA) and the free doxorubicin in the supernatant were isolated and quantified by measuring the absorption of doxorubicin at 480 nm with a microplate reader (TECAN, Infinite M200, Switzerland). The doxorubicin loading content and efficiency of loading into the DNA nanocarriers were calculated as shown in Scheme 1.

### Scheme 1. Method To Calculate Doxorubicin Loading Content and Efficiency of Loading into DNA Nanocarriers

$$\begin{aligned} \text{The final loading content of dox/origami} &= \text{Dox adding content at the beginning} - \text{Unloaded Dox in the supernatant} \\ \text{The loading efficiency of dox/origami} &= \frac{\text{The final loading content of dox/origami}}{\text{Dox adding content at the beginning}} \times 100\% \end{aligned}$$

The drug-loaded origami were then redissolved in PBS to form a stock solution (1 mM doxorubicin and  $\sim$ 1.25 nM origami) and diluted by no-serum cell culture medium for cellular experiments with a final doxorubicin concentration ranging from 5 to 100  $\mu\text{M}$ .

**Cells.** MCF 7 is a human breast adenocarcinoma cancer cell line. The doxorubicin-resistant MCF 7 cell subline was obtained by exposing regular MCF 7 cells to increasing amounts of doxorubicin. Both MCF 7 sublines were purchased from the Cell Center at the Institute of Basic Medical Sciences, Chinese Academy of Medical Science.

Regular MCF 7 cells were cultured in Dulbecco's Modified Eagle Medium, while the resistant subline was cultured in RPIM 1640 medium (Hyclone, Thermo Scientific). Both media were supplemented with 10% fetal bovine serum (Hyclone, Thermo Scientific) and with L-glutamine, penicillin, and streptomycin (GIBICO, Invitrogen). All the cells were cultured in an atmosphere of 5% CO<sub>2</sub> at 37 °C.

**Cell Viability Assay.** The cytotoxicity of doxorubicin origami was assessed by using a cell-counting kit (cck-8, Dojindo) which contained a highly water-soluble tetrazolium salt, WST-8 [2-(2-methoxy-4-nitrophenyl)-3-(4-nitrophenyl)-5-(2,4-disulfophenyl)-2H-tetrazolium, monosodium salt]. After seeding in 96-well plates and culturing overnight, the cells were incubated with doxorubicin, doxorubicin-triangle and doxorubicin-tube origami structures, and doxorubicin–ds M13 DNA (with a final doxorubicin concentration ranging from 5 to 100  $\mu\text{M}$ , diluted by serum-free culture media) for 12 h, and then washed with PBS and cultured for 24, 36, or 48 h. The cells were incubated with fresh serum-free medium containing 0.5 mg/mL WST-1 for 1 h at 37 °C for the cytotoxicity assay. The absorbance at 450 nm was measured using a microplate reader. For dead-cell staining, the res-MCF 7 cells were seeded and cultured overnight, treated with doxorubicin (100  $\mu\text{M}$ ), doxorubicin-triangle and doxorubicin-tube structures, and doxorubicin–ds M13 DNA (100  $\mu\text{M}$  loaded doxorubicin) for 12 h, and then washed with PBS and cultured for 48 h. SYTOX Green nucleic acid stain (Invitrogen, S7020) was only used for staining dead cells. The cells were incubated with SYTOX Green (10  $\mu\text{M}$ ) for 20 min at 37 °C and imaged directly by fluorescence microscopy (Leica, DMI 3000). A concentration of 125 pM (equivalent to the highest concentration of doxorubicin origami used in our study) of DNA origami structures was used in origami-only cell viability experiments. To obtain optimal qualitative results, we used a Hoechst/propidium iodide (PI, Dojindo) double stain and cell-counting kit. For cell-staining assays, both MCF 7 cell lines were seeded and treated with origami (triangle or tube) after culturing overnight for 12 h; they were subsequently washed with PBS and cultured for 48 h. The cells were then incubated with Hoechst 33342

(25  $\mu\text{g}/\text{mL}$ ) and PI (10  $\mu\text{g}/\text{mL}$ ) for 20 min at 37  $^{\circ}\text{C}$ . After being washed with PBS, the cells were examined and imaged by fluorescence microscopy.

**Co-localization of Doxorubicin and DNA Origami.** Reg-MCF 7 cells were seeded in confocal dishes, cultured overnight, and then incubated with purified FAM-labeled DNA origami (25 pM), doxorubicin (20  $\mu\text{M}$ ), and drug-loaded FAM-origami (loaded doxorubicin at 20  $\mu\text{M}$ , labeled origami  $\sim 25$  pM) for 24 h. After being washed with PBS, the living cells were visualized by laser confocal fluorescent microscopy (Zeiss).

**Doxorubicin Internalization.** Regular and drug-resistant MCF 7 cells were seeded in 96-well-plates and then cultured for 24 h. After adhesion, cells were incubated with doxorubicin, doxorubicin-triangle, and doxorubicin-tube structures at the same concentration (20, 50, and 100  $\mu\text{M}$ ) for 24 h. All the images were collected by a fluorescence microscope (Leica, DMI3000) and analyzed by a Leica IMAGE version workstation. For flow cytometry analysis of doxorubicin uptake, the cells were seeded and incubated with drug and drug-loaded carriers (20, 50, and 100  $\mu\text{M}$ ) for 24 h after adhesion. The cells were subsequently washed with PBS and harvested. All the treated cells were analyzed by a BD FACS Calibur flow cytometry system (BD Bioscience). Single fluorescent samples were used to optimize instrument settings and ensure proper electronic compensation.

**Lysosome Function Assay.** For studying the dynamic aspects of lysosome biogenesis and function in doxorubicin-sensitive and -resistant MCF 7 cells, LysoSensor and LysoTracker probes (Invitrogen) were used. Briefly, doxorubicin-sensitive and -resistant MCF 7 cells were seeded and cultured for 24 h. After incubation with free doxorubicin, doxorubicin-triangle, and doxorubicin-tube structures for 6 h, the cells were stained by LysoTracker Red DND-99 (1  $\mu\text{M}$ , diluted by serum-free medium) or LysoSensor Green DND-189 (fluorescent pH indicator, 2  $\mu\text{M}$ , diluted by serum-free medium) for 40 min. For co-localization of DNA origami and lysosomes, images were obtained with a laser confocal fluorescent microscopy (Zeiss). For the lysosome functional assay, images were obtained with a fluorescence microscope (Leica, DMI3000), and the fluorescent intensities were detected and analyzed by Beckman Coulter Cell Lab Quanta flow cytometry.

## RESULTS

**DNA Nanocarrier Design.** Two different DNA origami nanostructures, a 2D triangular structure and a 3D tubular structure, were used independently to deliver doxorubicin into tumor cells (Figure 1). After the doxorubicin was loaded into

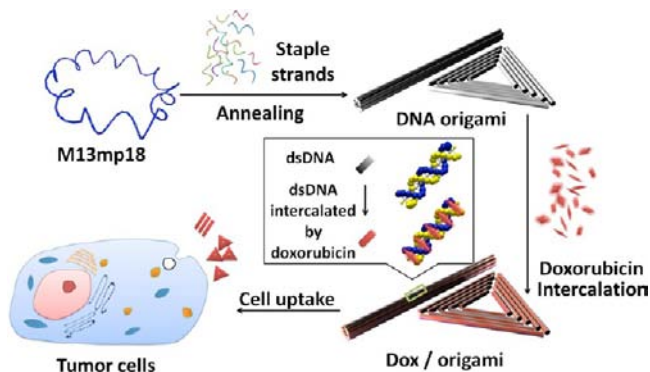


**Figure 1.** DNA origami and doxorubicin origami delivery system assembly. The long single-strand M13mp18 genomic DNA scaffold strand (blue) is folded into the triangle and tube structures through the hybridization of rationally designed staple strands. Watson–Crick base pairs in the double helices serve as docking sites for doxorubicin intercalation. After incubation with doxorubicin, the drug-loaded DNA nanostructure delivery vessels were administered to MCF 7 cells, and the effects were investigated.

the DNA nanocarriers through intercalation, MCF 7 cells were treated with the complexes. For both reg-MCF 7 and res-MCF 7 cell lines, the cytotoxicity of the nanocarrier–drug complexes was evaluated and compared to that of free doxorubicin at the same concentration (ranging from 5 to 100  $\mu\text{M}$ ).

**Loading DNA Origami Nanocarriers.** The DNA origami nanostructures were assembled through a single-step annealing process according to methods reported by Rothmund and Yan.<sup>13,36</sup> They were subsequently characterized, before and after drug loading, by agarose gel electrophoresis (AGE) and atomic force microscopy (AFM). As shown in the agarose gel image in Figure 2a, both the triangle- and tube-shaped origami structures migrated as sharp bands before incorporation of doxorubicin. After drug loading, both DNA carriers exhibited slight shifts in mobility, indicating that the doxorubicin was intercalated in the DNA. AFM images before and after drug loading provide direct evidence that the morphology of the nanostructures was retained after incorporation of the drug (Figure 2b). Doxorubicin can be visualized by its red fluorescence (520–660 nm, two peaks at 550 and 580 nm) when excited by a 488 nm argon ion laser or any other 450–490 nm light.<sup>1,37</sup> The efficiency of doxorubicin intercalation was determined by measuring the absorption at 480 nm and was shown to gradually increase with time (Figure 2c). After incubation of the DNA nanostructures with doxorubicin for 24 h at room temperature, approximately 50–60% of the drug was loaded in the structures. The unstructured dsDNA, M13 RF I DNA, was also used to load doxorubicin. Its loading efficiency was lower than that of DNA origami carriers, approximately 30% after 24 h incubation (Figure 2c).

### Cytotoxicity of Doxorubicin-Loaded DNA Origami.

We compared the cytotoxicity of free doxorubicin on the MCF 7 cell line to that of both doxorubicin origami complexes. Res-MCF 7 cells were obtained by exposure to increasing concentrations of doxorubicin. The resistance of the cells to doxorubicin was confirmed with a cell-counting kit (cck-8, see Methods for details) for a cell viability assay (Figure S1).

In the cytotoxicity experiments, reg-MCF 7 and res-MCF 7 cells were treated following exactly the same protocol. SYTOX Green, a green-fluorescent reporter molecule with a high affinity for nucleic acids, was used to indicate the presence of dead cell nuclei within a population (SYTOX Green is impermeable to live cells). For reg-MCF 7 cells, three experimental groups (free doxorubicin, doxorubicin-triangle, and doxorubicin-tube) induced cell death with no significant differences in cytotoxicity when the doxorubicin concentration was above 20  $\mu\text{M}$ , while free doxorubicin was slightly better than the origami loading system, and doxorubicin–ds M13 DNA did not induce effective cytotoxicity when the concentration was lower than 20  $\mu\text{M}$  (Figure S2a,b).

In contrast, free doxorubicin and doxorubicin-loaded unstructured dsDNA were insufficient to kill res-MCF 7 cells, while both the doxorubicin triangle and tube structures stimulated dramatically enhanced cell death, as shown in bright-field and fluorescence images of the SYTOX Green-stained cell nucleus, which also indicated nuclear-localized doxorubicin (Figures 3 and S2c).

To examine the effect of the DNA nanostructures themselves on both MCF 7 cell sublines, we administered drug-free DNA origami carriers to the cells. No obvious cytotoxicity to either cell phenotype was observed after 48 h incubation (Figure S3). For res-MCF 7 cells, the prominent characteristics of cell death were observed after 24, 36 (Figure S2c), and 48 h (Figure 3)

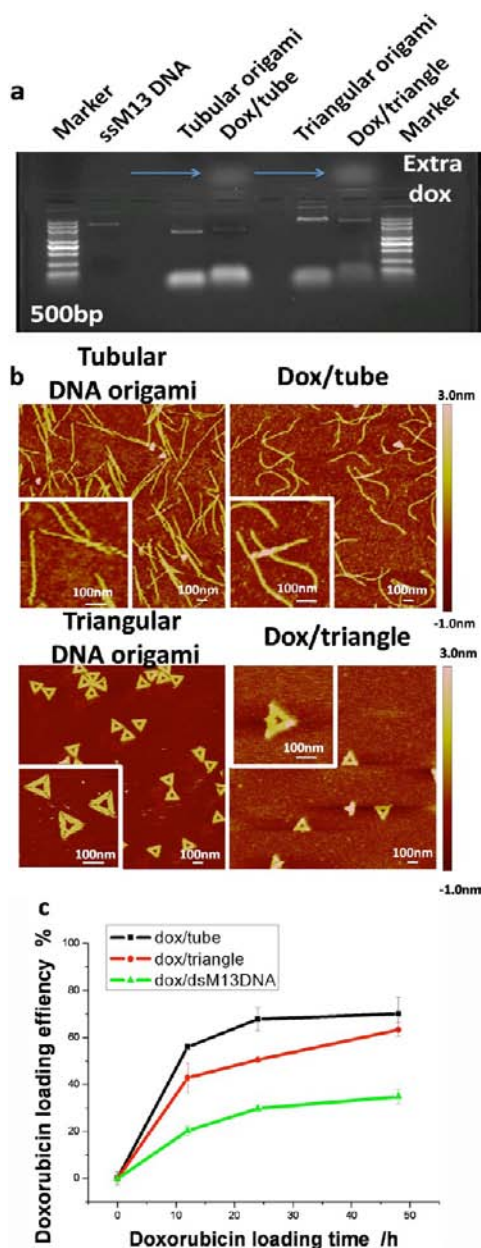


**Figure 2.** Characterization of DNA origami structures and drug loading efficiencies. (a) Ethidium bromide-stained agarose gel image of DNA origami and doxorubicin-loaded DNA structures. The blue arrows indicate the extra doxorubicin from drug-loaded DNA origami structures. (b) AFM images of DNA origami and after doxorubicin intercalation (scale bars are 100 nm). (c) Efficiency of doxorubicin incorporation into triangle- and tube-shaped DNA origami carriers and double-strand M13 DNA. Due to the large number of Watson–Crick base pairs in each structure, the drug loading efficiency is approximately 50–60% for DNA origami carriers and ~30% for double-strand M13 DNA after 24 h incubation at room temperature. Error bars represent standard deviation of three independent experiments in triplicate tubes of different doxorubicin-loaded DNA samples (tube, triangle, double-strand).

incubation with origami-bound doxorubicin structures. The cell-killing ability of the DNA nanostructure delivery vehicles exhibited dependence on both incubation time and concentration. The results suggest that DNA nanostructure-based drug delivery can potentially circumvent the development of drug resistance.

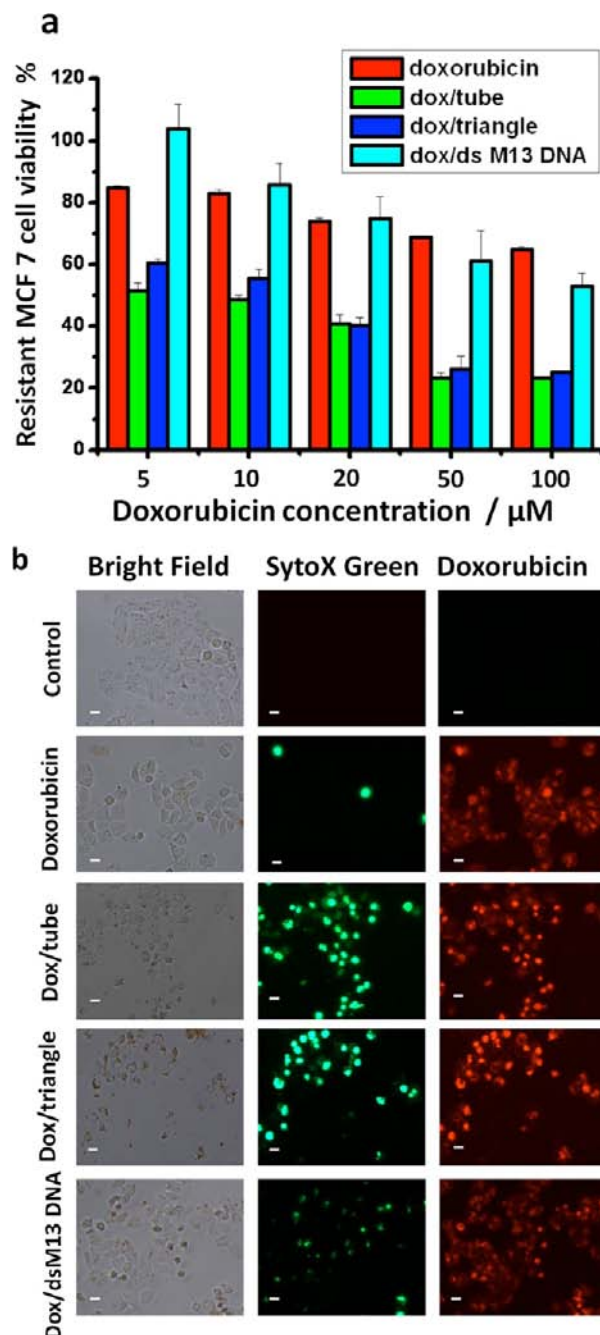


**Figure 3.** Cytotoxicity of doxorubicin-loaded DNA origami. (a) Cell viability of doxorubicin res-MCF 7 cells after administration with equal concentrations of free doxorubicin and drug-loaded origami for 48 h. Error bars represent standard deviation of three independent experiments in triplicate wells of cells. (b) Bright-field and fluorescence images of SYTOX Green dye (invitrogen) stained res-MCF 7 cells treated with 100  $\mu\text{M}$  free doxorubicin, doxorubicin-triangle and doxorubicin-tube structures (with 100  $\mu\text{M}$  doxorubicin), doxorubicin–ds M13 DNA, and vehicle solvent (control) for 48 h. Scale bars are 20  $\mu\text{m}$ . Both doxorubicin-triangle and doxorubicin-tube structure treated cells showed co-localization of drug and nuclei. The camera exposure times were 35.6 and 179.7 ms for SYTOX Green dye and doxorubicin, while the gains were 3.7 and 4.5, respectively. The images reveal that doxorubicin-loaded DNA origami structures are more effective at killing res-MCF 7 cells than free doxorubicin and doxorubicin-loaded dsDNA.

**Cellular Distribution of Doxorubicin Origami.** To study the cellular localization of the origami–doxorubicin complexes, res-MCF 7 cells were incubated with fluorescently labeled (fluorescein, green fluorescence) DNA origami (FAM-origami), free doxorubicin, and drug-loaded FAM origami, respectively. For many cell lines, even drug-resistant variants, doxorubicin can diffuse directly through intact cell membranes.<sup>1–3,38,39</sup> After 24 h incubation, the living cells were observed by confocal microscopy. Green fluorescence is visible inside cells that were treated with FAM-origami only, demonstrating that the bare FAM-origami nanocarriers can enter and accumulate in cells (Figure 4). For cells treated with free doxorubicin, intracellular

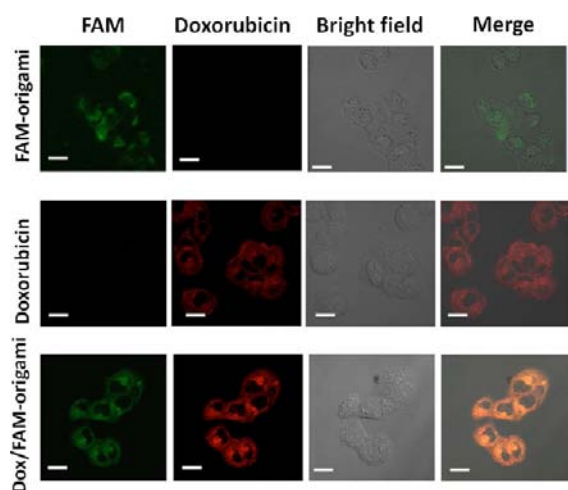


**Figure 4.** Co-localization of doxorubicin- and FAM-labeled DNA origami in drug-resistant MCF 7 cells. Fluorescence images of FAM-labeled DNA origami (125 pM), doxorubicin (20  $\mu$ M), and doxorubicin-loaded FAM-origami (20  $\mu$ M loaded doxorubicin, 125 pM FAM-origami) incubated with res-MCF 7 cells for 24 h. Scale bars are 20  $\mu$ m. Laser intensities of 488 nm and 514 nm were 25% and 15%, and digital gain was 1.00.

red fluorescence was observed. The confocal images in Figure 4 show overlapping green (FAM-origami) and red (doxorubicin) fluorescence signals corresponding to the cellular co-localization of FAM-origami and doxorubicin, respectively. The results confirm that the origami nanocarriers can effectively deliver the drugs into living cells.

**Intracellular Accumulation of Doxorubicin Origami and Circumvention of Drug Resistance.** To determine if enhanced cellular doxorubicin accumulation contributes to the ability of the DNA origami-based drug delivery system to circumvent drug resistance in res-MCF 7 cells, flow cytometry and confocal fluorescent analysis were performed. Both MCF 7 cell phenotypes were incubated with equal concentrations of free doxorubicin, doxorubicin-triangle, and doxorubicin-tube complexes for 24 h and subsequently analyzed. Res-MCF 7 cells treated with the doxorubicin–DNA origami exhibited much stronger red fluorescence (doxorubicin) than those treated with free doxorubicin at the same concentration (Figures 5a,b and S4a). In comparison, no significant differences in doxorubicin internalization were observed among reg-MCF 7 cells (Figure S4b). These results suggest that the DNA nanostructure delivery system is capable of circumventing drug resistance in res-MCF 7 cells by facilitating efficient intracellular accumulation of the drug.

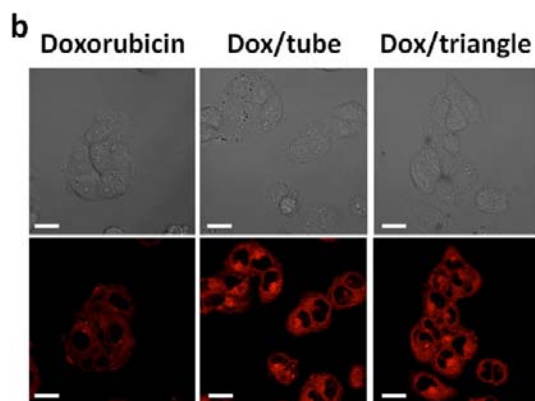
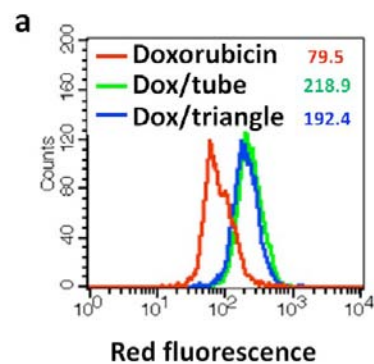


**Figure 5.** Doxorubicin internalization. (a) Flow cytometry analysis of drug-resistant MCF 7 cells that were incubated with 20  $\mu$ M doxorubicin, doxorubicin-triangle, and doxorubicin-tube structures for 24 h. The PMT voltage of the red fluorescence channel was 3.75, and the gain was 2.00. The mean values of red channel fluorescence are shown as numbers in the histograms. (b) Confocal fluorescence images of the same samples. Scale bars are 20  $\mu$ m. The lasers intensity of 488 nm was 10%, and digital gain was 1.00. The average fluorescence intensity of cells treated with doxorubicin origami is higher than that of cells treated with free doxorubicin, indicating that the DNA origami delivery vehicle increases the amount of doxorubicin internalized.

**Inhibition of Lysosomal Acidification.** Many anti-cancer drugs, including doxorubicin, are classified as weak bases whose activity inside cells is pH dependent. In drug-resistant cells, these therapeutic agents tend to accumulate in the most acidic intracellular compartments, e.g., lysosomes, rather than being dispersed throughout the cytoplasm and nucleus as in drug-sensitive cells. Studies have already shown that disrupting the pH of acidic intracellular organelles in resistant cells can reverse drug resistance.<sup>40–42</sup> DNA origami was labeled with fluorescent dye, FAM, to check its intracellular distribution after 6 h treatment, and the samples were analyzed by laser confocal microscopy. Confocal images showed the fluorescence signal of FAM partially overlapped with that of LysoTracker Red after 6 h incubation with res-MCF 7 cells (Figure 6a), suggesting the endocytosis of FAM-labeled DNA origami carriers and localization of origami nanostructures in lysosomes at the treatment time point of 6 h.

To evaluate the influence of doxorubicin origami structures on lysosomal pH and determine if these effects contribute to the observed circumvention of drug resistance, a LysoSensor Green probe was employed. This probe is pH sensitive and exhibits weaker fluorescence at higher pH. Res-MCF 7 cells were incubated with doxorubicin origami for 6 h and subsequently stained with the lysosome-specific probe.

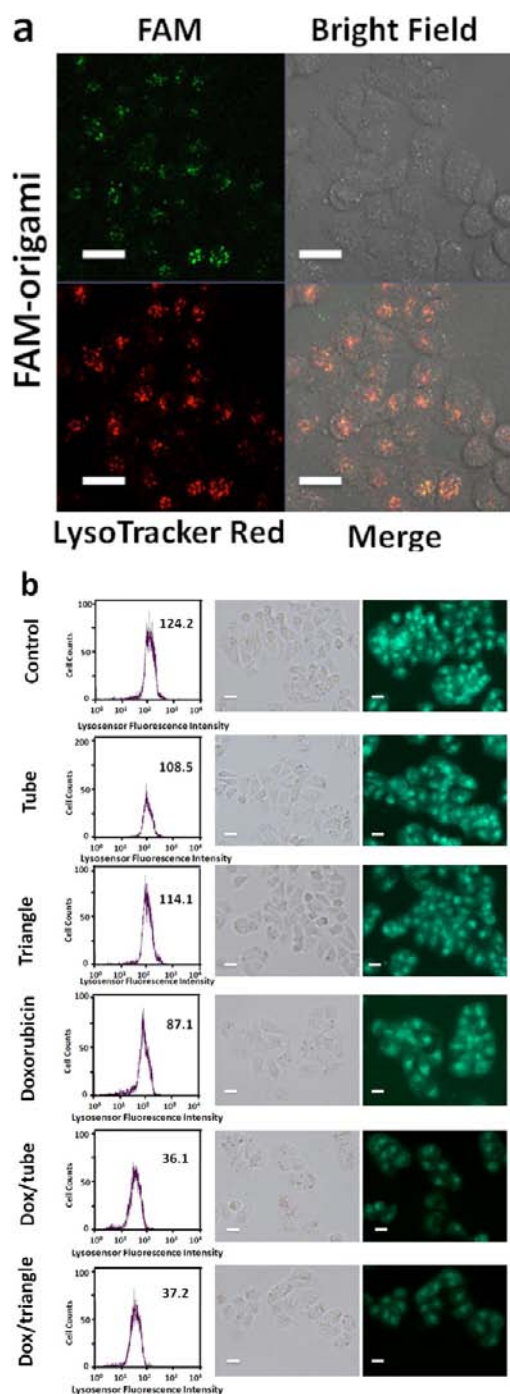


**Figure 6.** Lysosomal function assay. (a) Co-localization of lysosomes and FAM-labeled DNA origami in drug-resistant MCF7 cells. Fluorescence images of FAM-labeled DNA origami (125pM) incubated with res-MCF7 cells for 6 h and then stained with LysoTracker Red DND-99. Scale bars are 20  $\mu\text{m}$ . The laser intensity of 488 and 543 nm was 25%, and digital gain was 1.00. (b) Fluorescence images of LysoSensor Green DND-169 probe-stained res-MCF7 cells after 6 h incubation with 100  $\mu\text{M}$  doxorubicin and drug-loaded DNA. The camera exposure time was 23.2 ms, and the gain was 3.0. Scale bars are 20  $\mu\text{m}$ . The fluorescence intensities were detected and analyzed by Beckman Coulter Cell Lab Quanta flow cytometry, which illustrates the LysoSensor Green fluorescence intensity of cells treated with different structures. The PMT voltages of the green fluorescence channel were 3.20, and the gain was 4.00. The mean values of green channel fluorescence are shown as numbers in the histograms.

Resistant cells treated with doxorubicin-triangle and doxorubicin-tube structures exhibited weaker green fluorescence than cells treated with free doxorubicin only (Figure 6b), signifying a higher pH and stronger inhibition of lysosomal acidification.

For reg-MCF7 cells, both free doxorubicin and doxorubicin origami structures showed decreased green fluorescence, with no significant differences in fluorescence intensity among the groups (Figure S5). In particular, there was no difference in lysosomal pH for cells treated with bare origami structures (triangle and tube) compared to those treated with solvent only (control), suggesting that lysosomal pH was not affected by the DNA nanostructures themselves (Figures 6 and S5).

## DISCUSSION

We demonstrated a biocompatible drug carrier system based on spatially addressable DNA origami nanostructures (triangle and tube structures). Doxorubicin, a well-known chemotherapy drug, was efficiently loaded into the large DNA assemblies, and the doxorubicin-loaded structures were administered to drug-sensitive and drug-resistant phenotypes of MCF7 human breast adenocarcinoma cancer cells. Confocal fluorescent analyses confirmed that the doxorubicin origami structures are effectively internalized by tumor cells and that the signals from both components (the drug and the carrier) are co-localized in the cytoplasm after 24 h treatment (Figure 4). Free doxorubicin and the doxorubicin origami complexes were both effective at inducing cell death in the regular, doxorubicin-sensitive MCF7 cell line. However, free doxorubicin and doxorubicin-loaded dsDNA were not effective at killing resistant MCF7 cells, while the same concentration of origami-bound doxorubicin induced cell death. These results suggest that DNA nanostructure carriers have the potential to circumvent doxorubicin resistance.

Further, we considered the means by which drug-loaded DNA nanostructures circumvent resistance in res-MCF7 cells. Generally speaking, cultured cancer cells can become resistant to cytotoxic anti-cancer drugs in many ways.<sup>4,5</sup> One of the most common ways is decreased internalization of the drugs by cells. For example, some tumor cells express high levels of membrane efflux pumps that can eject drugs or decrease drug uptake; clinical and laboratory studies have suggested that increasing the amount of drug that is internalized, by suppressing efflux pumps, for example, can overcome drug resistance.<sup>5</sup> We tried another widely used drug carrier, PEG-PLA (poly(ethylene glycol)-poly(lactic-co-glycolic acid)) copolymer micelles, to check their cytotoxicity for comparison (Figure S6). PEG-PLA micelles were assembled by a double-emulsion method,<sup>43,44</sup> and the diameter was  $215.3 \pm 0.5$  nm. Reg-MCF7 showed obvious cytotoxicity after treatment with both doxorubicin alone and doxorubicin micelles. However, there was no obvious cytotoxicity in the res-MCF7 cells for both doxorubicin alone and doxorubicin micelles. Based on this result, we assume the uptake effect is size and shape dependent; flow cytometry and fluorescent confocal analysis revealed that the DNA origami carriers did enhance the cellular uptake of doxorubicin in res-MCF7 cells and were involved in the circumvention of drug resistance.

The development of multidrug resistance in tumor cells is also related to intracellular pH, both in the cytoplasm and in acidic organelles.<sup>40</sup> In tumor cells displaying resistant phenotype, anti-cancer drugs are restricted to acidic organelles such as lysosomes and do not reach their sites of action in the cytosol and nucleus.<sup>3</sup> Studies have shown that increasing

lysosomal pH in resistant tumor cells with lysosomotropic agents disrupts compartmentalization and redistributes the drug to active sites.<sup>41,42</sup> Here, lysosomal function studies revealed that doxorubicin-resistant MCF 7 cells treated with drug-loaded DNA origami structures exhibited elevated pH, indicating inhibition of lysosomal acidification. Taken together, the results indicate that the DNA nanostructure delivery platform circumvents drug resistance in res-MCF 7 cells by increasing the cellular uptake of doxorubicin and inducing a change in lysosomal pH that redistributes the drug to target sites.

Despite being slowly digested by enzymes in the cell, DNA nanocarriers are themselves biological molecules that do not pose the same health risks as metal NP delivery systems. Others have demonstrated that, in the absence of specific immunostimulating oligonucleotides, the intrinsic immunogenicity of DNA origami did not increase significantly compared to levels in untreated groups (in fresh isolated spleen cells and macrophage-like Raw264.7 cell line and in tumor xenograft mice).<sup>31,33,45</sup> Thus, DNA origami represents a nontoxic, biocompatible drug delivery system. Loaded drug can be released through slow degradation of DNA nanostructures by low environmental pH values or DNA enzymes (Figure S7), which suggest the potential of controlled drug release. Modifying the DNA nanostructure surface with precise three-dimensional arrangements of imaging labels or multiple target groups such as peptides or antibodies can improve the activity and functionality of the delivery vehicles. Moreover, several different anti-cancer drugs, small molecules, and siRNA could be simultaneously delivered to cells for synergistic therapy. We believe that DNA origami has immense potential as an efficient, biocompatible drug carrier and delivery vehicle in the treatment of cancer.

## ■ ASSOCIATED CONTENT

### ● Supporting Information

Extra figures and microscopy images. This material is available free of charge via the Internet at <http://pubs.acs.org>.

## ■ AUTHOR INFORMATION

### Corresponding Author

dingbq@nanoctr.cn; hao.yan@asu.edu

### Notes

The authors declare no competing financial interest.

## ■ ACKNOWLEDGMENTS

The authors are grateful for financial support from National Basic Research Program of China (973 Program, 2012CB934000), 100-Talent Program of Chinese Academy of Sciences (B.D.), National Science Foundation China (21173059, 91127021), Beijing Natural Science Foundation (2122057), and the U.S. National Institutes of Health. The authors thank Prof. Yan Wu for kindly providing PEG-PLA micelles and Yun Sun for helpful discussions.

## ■ REFERENCES

- (1) Pigyam, W. J.; Filler, W.; Hamilton, L. D. *Nat. New Biol.* **1972**, 235, 17–19.
- (2) Hortobagyi, G. N. *Drugs*. **1997**, 54 (suppl. 4), 1–7.
- (3) Wadler, S.; Fuks, J. Z.; Wiernik, P. H. *J. Clin. Pharmacol.* **1987**, 27, 357–365.
- (4) Pastan, I.; Gottesman, M. M. *Annu. Rev. Med.* **1991**, 42, 277–286.
- (5) Gottesman, M. M. *Annu. Rev. Med.* **2002**, 53, 615–627.
- (6) Petros, R. A.; DeSimone, J. M. *Nat. Rev. Drug Discov.* **2010**, 9, 615–627.
- (7) Davis, M. E.; Chen, Z. G.; Shin, D. M. *Nat. Rev. Drug Discov.* **2008**, 7, 771–782.
- (8) Heath, J. R.; Davis, M. E. *Annu. Rev. Med.* **2008**, 59, 251–265.
- (9) Wang, A. Z.; Langer, R.; Farokhzad, O. C. *Annu. Rev. Med.* **2012**, 63, 185–198.
- (10) Allen, T. M.; Mumbengegwi, D. R.; Charrois, G. J. *Clin. Cancer Res.* **2005**, 11, 3567–3573.
- (11) Bandak, S.; Goren, D.; Horowitz, A.; Tzemach, D.; Gabizon, A. *Anticancer Drugs* **1999**, 10, 911–920.
- (12) Minelli, C.; Lowe, S. B.; Stevens, M. M. *Small* **2010**, 6, 2336–2357.
- (13) Rothmund, P. W. K. *Nature* **2006**, 440, 297–302.
- (14) Seeman, N. C. *J. Theor. Biol.* **1982**, 99, 237–247.
- (15) Winfree, E.; Liu, F.; Wenzler, L. A.; Seeman, N. C. *Nature* **1998**, 394, 539–544.
- (16) LaBean, T. H.; Yan, H.; Kopatsch, J.; Liu, F.; Winfree, E.; Reif, J. H.; Seeman, N. C. *J. Am. Chem. Soc.* **2000**, 122, 1848–1860.
- (17) Yan, H.; Park, S. H.; Finkelstein, G.; Reif, J. H.; LaBean, T. H. *Science* **2003**, 301, 1882–1884.
- (18) Goodman, R. P.; Berry, R. M.; Turberfield, A. J. *Chem. Commun.* **2004**, 12, 1372–1373.
- (19) Erben, C. M.; Goodman, R. P.; Turberfield, A. J. *J. Am. Chem. Soc.* **2007**, 129, 6992–6993.
- (20) Andersen, E. S.; Dong, M.; Nielsen, M. M.; Jahn, K.; Subramani, R.; Mamdouh, W.; Golas, M. M.; Sander, B.; Stark, H.; Oliveira, C. L. P.; Pedersen, J. S.; Birkedal, V.; Besenbacher, F.; Gothelf, K. V.; Kjems, J. *Nature* **2009**, 459, 73–77.
- (21) Douglas, S.; Dietz, H.; Liedl, T.; Högberg, B.; Graf, F.; Shih, W. *Nature* **2009**, 459, 414–418.
- (22) Dietz, H.; Douglas, S. M.; Shih, W. M. *Science* **2009**, 325, 725–730.
- (23) Liedl, T.; Högberg, B.; Tytell, J.; Ingber, D. E.; Shih, W. M. *Nat. Nanotechnol.* **2010**, 5, 520–524.
- (24) Han, D.; Pal, S.; Nangreave, J.; Deng, Z.; Liu, Y.; Yan, H. *Science* **2011**, 332, 342–346.
- (25) Ding, B. Q.; Deng, Z. T.; Yan, H.; Cabrini, S.; Zuckermann, R. N.; Bokor, J. *J. Am. Chem. Soc.* **2010**, 132, 3248–3249.
- (26) Pal, S.; Deng, Z.; Ding, B. Q.; Yan, H.; Liu, Y. *Angew. Chem., Int. Ed.* **2010**, 49, 2700–2704.
- (27) Pal, S.; Varghese, R.; Yan, H.; Liu, Y. *Angew. Chem., Int. Ed.* **2011**, 50, 4176–4179.
- (28) Ding, B.; Wu, H.; Xu, W.; Zhao, Z.; Liu, Y.; Yu, H.; Yan, H. *Nano Lett.* **2010**, 10, 5065–5069.
- (29) Voigt, N. V.; Tørring, T.; Rotaru, A.; Jacobsen, M. F.; Ravnsbæk, J. B.; Subramani, R.; Mamdouh, W.; Kjems, J.; Mokhir, A.; Besenbacher, F.; Gothelf, K. V. *Nat. Nanotechnol.* **2010**, 5, 200–203.
- (30) Pinheiro, A. V.; Han, D.; Shih, W. M.; Yan, H. *Nat. Nanotechnol.* **2011**, 6, 763–772.
- (31) Schüller, V. J.; Heidegger, S.; Sandholzer, N.; Nickels, P. C.; Suhartha, N. A.; Endres, S.; Bourquin, C.; Liedl, T. *ACS Nano* **2011**, 5, 9696–9702.
- (32) Douglas, S. M.; Bachelet, I.; Church, G. M. *Science* **2012**, 335, 831–834.
- (33) Li, J.; Pei, H.; Zhu, B.; Le Liang, L.; Min Wei, M.; Yao, He, Y.; Nan Chen, N.; Di Li, D.; Qing Huang, Q.; Fan, C. *ACS Nano* **2011**, 5, 8783–8789.
- (34) Huang, D. M.; Chang, M.; Yang, C. S. *ACS Nano* **2011**, 5, 6156–6163.
- (35) Mei, Q.; Wei, X.; Su, F.; Liu, Y.; Youngbull, C.; Johnson, R.; Lindsay, S.; Yan, H. *Nano Lett.* **2011**, 11, 1477–1482.
- (36) Stearns, L. A.; Chhabra, R.; Sharma, J.; Liu, Y.; Petuskey, W. T.; Yan, H.; Chaput, J. C. *Angew. Chem., Int. Ed.* **2009**, 45, 8646–8648.
- (37) Anderson, A. B.; Gergen, J.; Arriaga, E. A. *J. Chromatogr. B* **2002**, 769, 97–106.
- (38) Dalmark, M.; Storm, H. H. *J. Gen. Physiol.* **1981**, 78, 349–364.

- (39) Sardini, A.; Mintenig, G. M.; Valverde, M. A.; Sepulveda, F. V.; Gill, D. R.; Hyde, S. C.; Higgins, C. F.; McNaughton, P. A. *J. Cell. Sci.* **1994**, *107*, 3281–3290.
- (40) Schindler, M.; Grabski, S.; Hoff, E.; Simon, S. M. *Biochemistry.* **1996**, *35*, 2811–2817.
- (41) Simon, S. M.; Altan, N.; Chen, Y.; Schindler, M. *Proc. Natl. Acad. Sci. U.S.A.* **1999**, *96*, 4432–4437.
- (42) Hurwitz, S. J.; Terashima, M.; Mizunuma, N.; Slapak, C. A. *Blood* **1997**, *89*, 3745–3754.
- (43) Lee, E. S.; Naa, K.; Baea, Y. H. *J. Controlled Release* **2003**, *91*, 103–113.
- (44) Kim, D.; Lee, E. S.; Oh, K. T.; Gao, Z. G.; Baea, Y. H. *Small* **2008**, *4*, 2043–2050.
- (45) Lee, H.; Lytton-Jean, A. K. R.; Chen, Y.; Love, K. T.; Park, A. I.; Karagiannis, E. D.; Sehgal, A.; Querbes, W.; Zurenko, C. S.; Jayaraman, M.; Peng, C. G.; Charisse, K.; Borodovsky, A.; Manoharan, M.; Donahoe, J. S.; Truelove, J.; Nahrendorf, M.; Langer, R.; Anderson, D. G. *Nat. Nanotechnol.* **2012**, *7*, 389–393.